J|A|C|S
ARTICLES
Published on Web 12/09/2006

Electrochemical Oxidation of $CoCp(CO)_2$: Radical−Substrate Reaction of a 17 e^-/18 e^- Pair and Production of a Unique Dimer Radical

Ayman Nafady,[†,§] Paulo Jorge Costa,[‡] Maria José Calhorda,*[,‡] and William E. Geiger*[,†]

Contribution from the Department of Chemistry, University of Vermont, Burlington, Vermont 05405, and Departamento de Química e Bioquímica, Faculdade de Ciências, Universidade de Lisboa, 1749-016 Lisboa, Portugal and Instituto de Tecnologia Química e Biológica, Av. da República, EAN, Apart. 127, 2781-901 Oeiras, Portugal

Received July 26, 2006; E-mail: William.Geiger@UVM.edu; Ayman.Nafady@sci.monash.edu.au

Abstract: Anodic oxidation of the important half-sandwich compound $CoCp(CO)_2$, **1**, has been studied under gentle electrolyte conditions, e.g., chlorinated hydrocarbons with weakly coordinating anion (WCA) supporting electrolyte anions. The 17-electron cation $\mathbf{1}^+$ produced at $E_{1/2}(1) = 0.37$ V vs $FeCp_2^{0/+}$ undergoes a surprising reaction with neutral **1** to form the dimer radical cation $[Co_2Cp_2(CO)_4]^+$, $\mathbf{2}^+$, which has a metal−metal bond unsupported by bridging ligands. The dimer radical is oxidized at a slightly more positive potential ($E_{1/2} = 0.47$ V) to the corresponding dication $\mathbf{2}^{2+}$. Observation of the oxidation of $\mathbf{2}^+$ is without precedent in confirming a radical−substrate (R−S) dimerization process by direct voltammetric detection of the R−S intermediate, $K_{eq} = 3 \times 10^4$ M^{-1} for $[\mathbf{2}^+]/[\mathbf{1}][\mathbf{1}^+]$. The R−S mechanism and the reaction products have been characterized by voltammetry, electrolysis, fiber-optic IR spectroscopy, and ESR measurements. DFT calculations indicate that removal of an electron from **1** results in rehybridization in $\mathbf{1}^+$, thereby opening the metal center for interaction with the neutral compound **1**, which has a relatively basic metal center. The LUMO of the dimer dication $\mathbf{2}^{2+}$ is metal−metal antibonding, and its half-occupancy in $\mathbf{2}^+$ results in lengthening of the Co−Co bond from 2.64 Å to 3.14 Å. Inclusion of solvent in the (COSMO) calculations shows that solvation effects are necessary to account for the fact that $E_{1/2}(2) > E_{1/2}(1)$. These results show the importance of medium effects in probing the fundamental redox chemistry of half-sandwich metal complexes.

Introduction

Piano-stool metal carbonyl complexes with 18 electrons have played an important role in the historical and practical development of organometallic chemistry.[1,2] These "half-sandwich" complexes have the general formula (π-ArR)M(CO)$_n$, where (π-ArR) is a planar aromatic ligand, and n is the number of carbonyl groups necessary to achieve the inert-gas configuration. Although their 16 e^- /18 e^- chemistry is continuing to be productively exploited,[3] the 17 e^- chemistry of piano-stool radical cations is surprisingly underdeveloped. There is certainly a plethora of examples of stable, or at least persistent, 17 e^- radical cations containing a modified π- hydrocarbon and/or a different two-electron ligand which increases the thermodynamic and kinetic radical stabilities owing to greater electron density at the metal center.[4] Examples include the replacements of η^5-C_5H_5 (Cp) by η^5-C_5Me_5 (Cp*) and CO by a phosphine[4d] or isocyanide ligand. The consequent electronic and chemical properties of the radicals may, of course, differ significantly from those of their unsubstituted parents. Specifically, the latter are expected to be much more highly oxidizing[5] and to undergo more facile associative reaction pathways owing to the strong electron-withdrawing character and minimal steric encumbrance of the CO ligand.

We have sought to develop experimental conditions that would allow more general access to long-lived radical cations of the parent compounds. A number of them have been

[†] University of Vermont.
[‡] Universidade de Lisboa.
[§] Present address: School of Chemistry, Monash University, Clayton, Victoria 3800, Australia.

(1) Collman, J. P.; Hegedus, L. S.; Norton, J. R.; Finke, R. G. *Principles and Applications of Organotransition Metal Chemistry*, 2nd ed.; University Science Books: Mill Valley, CA, 1987; Chapter 3.
(2) Elschenbroich, Ch. *Organometallics*, 3rd ed.; VCH Publishers: Weinheim, 2005; esp. Chapter 15
(3) (a) Asbury, J. B.; Ghosh, H. N.; Yeston, J. S.; Bergman, R. G.; Lian, T. *Organometallics* **1998**, *17*, 3417 (b) Asplund, M. C.; Snee, P. T.; Yeston, J. S.; Wilkens, M. J.; Payne, C. K.; Yang, H.; Kotz, K. T.; Frei, H.; Bergman, R. G.; Harris, C. B. *J. Am. Chem. Soc.* **2002**, *124*, 10605 (c) Wang, X.; Wovchko, E. A. *J. Phys. Chem. B* **2005**, *109*, 16363 (d) Jina, O. S.; Sun, X. Z.; George, M. W. *J. Chem. Soc., Dalton Trans.* **2003**, 1773.
(4) (a) Connelly, N. G.; Geiger, W. E. In *Advances in Organometallic Chemistry*; Stone, F. G. A.; West, R., Eds; Academic Press: Orlando, FL, 1984; Volume 23, pp 1−93. (b) Baird, M. C. In *Organometallic Radical Processes*; Trogler, W. C., Ed.; Elsevier: Amsterdam, 1990; pp 49−66. (c) Astruc, D. *Electron Transfer and Radical Processes in Transition-Metal Chemistry*; VCH Publishers: New York, 1995. esp. Most relevant to the present paper are pp 198−203, 327, 425, 443, 461. (d) Orpen, A. G.; Connelly, N. G. *Organometallics* **1990**, *9*, 1206.
(5) A measure of this effect is the shift to more negative $E_{1/2}$ potentials for the oxidation of a metal carbonyl compound when a carbonyl group is replaced by another ligand. In the case of $Cr(CO)_5(PPh_3)$, the shift is −0.35 V (see Chatt, J.; Kan, C. T.; Leigh, G. J.; Pickett, C. J.; Stanley, D. R. *J. Chem. Soc., Dalton Trans.* **1980**, 2032). See also: Lever, A. B. P. *Inorg. Chem.* **1990**, *29*, 1271 and references therein.

previously shown to have transient existence, at least on the cyclic voltammetry (CV) time scale of ca. 10 s, including $[Cr(\eta^6\text{-benzene})(CO)_3]^+$ [6] and $[MnCp(CO)_3]^+$,[7] the latter in CF_3CO_2H. There was, apparently, no reliable description of a long-lived radical cation of this type, even as an in situ electrolysis product, prior to the reported spectral characterization of $[Cr(\eta^6\text{-benzene})(CO)_3]^+$ in CH_2Cl_2 containing the weakly coordinating anion (WCA)[8] *tetrakis*(perfluorophenyl)borate, $[B(C_6F_5)_4]^-$ or TFAB, which eliminated the nucleophilic attack on the radical by traditional electrolyte anions such as $[BF_4]^-$.[9] In that paper, we also reported the electrochemical generation of $[CoCp(CO)_2]^+$, $\mathbf{1}^+$, and suggested, based on CV data, that 17 e$^-$ $\mathbf{1}^+$ reacts with 18 e$^-$ **1** to produce the dimer radical cation $\mathbf{2}^+$. The

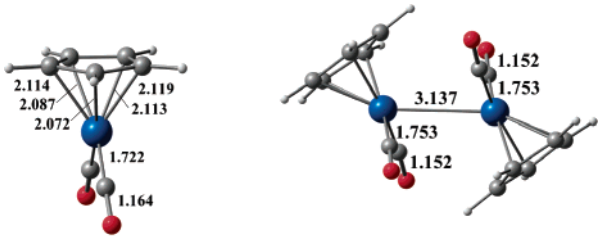

1 $\mathbf{2}^+$

proposed structure of $\mathbf{2}^+$, involving a metal−metal bond unsupported by bridging ligands, was unprecedented among radicals.[10] We now offer a more complete description of this unique system, including aspects of its structure (see above drawing) and bonding. As will be shown, medium effects (both solvation and ion pairing) play a key role in the formation and reactions of the cobalt and dicobalt radicals.

The mechanism proposed[9] for the formation of $\mathbf{2}^+$, namely the ECE mechanism of eqs 1−3, requires scrutiny. In this sequence, the oxidation of **1** to $\mathbf{1}^+$ (eq 1) is followed by the reaction of the radical with a second equivalent of starting material, **1**, to form the dimer radical $\mathbf{2}^+$ (eq 2). The latter is subsequently oxidized in a separate anodic wave to $\mathbf{2}^{2+}$ (eq 3).

$$CoCp(CO)_2 \rightleftharpoons [CoCp(CO)_2]^+ + e^- \qquad E_{1/2}(1) = 0.37\ \text{V} \quad (1)$$

$$\underset{\mathbf{1}^+}{[CoCp(CO)_2]^+} + \underset{\mathbf{1}}{CoCp(CO)_2} \underset{k_b}{\overset{k_f}{\rightleftharpoons}} \underset{\mathbf{2}^+}{[Co_2Cp_2(CO)_4]^+} \qquad K_{eq} = [\mathbf{2}^+]/[\mathbf{1}^+][\mathbf{1}] \quad (2)$$

$$\underset{\mathbf{2}^+}{[Co_2Cp_2(CO)_4]^+} \rightleftharpoons \underset{\mathbf{2}^{2+}}{[Co_2Cp_2(CO)_4]^{2+}} + e^- \qquad E_{1/2}(2) = 0.47\ \text{V} \quad (3)$$

Using terminology from the electrochemical literature, the dimer radical $\mathbf{2}^+$ is said to form through a radical−substrate (R−S) mechanism.[11] Although R−S mechanisms have been frequently invoked in both organic and inorganic redox dimerizations, they do not appear to have been confirmed by direct voltammetric observation of the $[R-S]^+$ intermediate, owing to its lack of thermodynamic stability under the applied potential at which it is formed. That is, for an oxidation process, $E_{1/2}(2)$ is generally *negative* of $E_{1/2}(1)$, and any $[R-S]^+$ formed would be oxidized by the electrode at a diffusion-controlled rate to the final dication, $[R-R]^{2+}$ as it is formed. In that circumstance, the CV scans observed for the R−S mechanism are virtually identical to those observed for the more commonly invoked radical−radical (R−R) mechanism, in that both show a *single* one-electron anodic wave (as S is oxidized to $^1/_2[R-R]^{2+}$) followed on the return by a two-electron cathodic wave for half an equivalent of $[R-R]^{2+}$ being reduced to S.[12] A simulated example is shown in Figure 1. In the context of half-sandwich complexes, this sort of CV behavior has been observed in the oxidations of $[MCp(CO)_3]^-$ (M = Mo, W) and $[FeCp(CO)_2]^-$ to the neutral dimers $M_2Cp_2(CO)_6$ and $Fe_2Cp_2(CO)_4$, respectively,[13] as well as in the oxidation of RhCp(CO)L, L = phosphine or phosphite, to the corresponding dimer dication.[14]

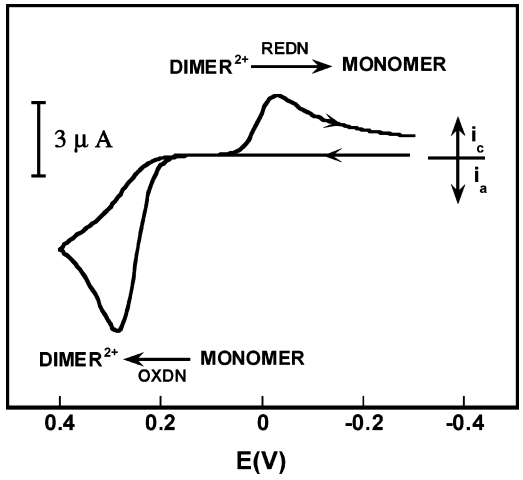

Figure 1. Simulated cyclic voltammogram showing a "normal" case in which a single anodic wave is observed for the oxidation of monomer to dimer dication, followed by a single cathodic wave for the reduction of the dication back to the neutral starting material. This CV shape is expected for a radical−radical coupling reaction or for a radical−substrate reaction in which $E_{1/2}(2)$ is less positive than $E_{1/2}(1)$ (see eqs 1 and 3 in text). For this simulation, an RS mechanism was employed with $E_{1/2}(1) = 0.30$ V, $\alpha_1 = 0.5$, $k_s^1 = 0.1$ cm/s, $E_{1/2}(2) = 0$ V, $\alpha_2 = 0.35$, $k_s^1 = 0.01$ cm/s, $K_{eq} = 3 \times 10^5$ M^{-1}, $k_{dim} = 1 \times 10^6$ M^{-1} s^{-1}, electrode area = 0.0078 cm^2, concn of monomer = 0.001 M.

(6) (a) Meng, Q.; Huang, Y.; Ryan, W. J.; Sweigart, D. A. *Inorg. Chem.* **1992**, *31*, 4051. (b) Zoski, C. G.; Sweigart, D. A.; Stone, N. J.; Rieger, P. H.; Mocellin, E.; Mann, T. F.; Mann, D. R.; Gosser, D. K.; Doeff, M. M.; Bond, A. M. *J. Am. Chem. Soc.* **1988**, *110*, 2109.
(7) Pickett, C. J.; Pletcher, D. *J. Chem. Soc., Dalton Trans.* **1976**, 636. The ESR spectrum assigned in this paper to $[MnCp(CO)_3]^+$, after bulk oxidation of the neutral complex ($A_{iso} = 92.5$ G), almost surely arises from a Mn(II) decomposition product.
(8) References to Weakly Coordinating Anions (WCAs): (a) Strauss, S. H. *Chem. Rev.* **1993**, *93*, 927. (b) Reed, C. A. *Acc. Chem. Res.* **1998**, *31*, 133. (c) Krossing, I. Raabe, I. *Angew. Chem., Int. Ed.* **2004**, *43*, 2066
(9) Camire, N.; Nafady, A.; Geiger, W. E. *J. Am. Chem. Soc.* **2002**, *124*, 7260
(10) We do not include multiply bonded metal−metal systems in this statement.
(11) For leading references to voltammetric studies of electron-transfer initiated dimerization reactions, see: Parker, V. D. *Acta Chem. Scand.* **1998**, *52*, 154. (b) Andrieux, C. P.; Grzeszczuk, M.; Savéant, J-M. *J. Electroanal. Chem.* **1991**, *318*, 369. (c) Alden, J. A.; Cooper, J. A.; Hutchinson, F.; Prieto, F.; Compton, R. G. *J. Electroanal. Chem.* **1997**, *432*, 63. (d) Amatore, C.; Pinson, J.; Savéant, J-M. *J. Electroanal. Chem.* **1982**, *137*, 143. (e) Andrieux, C. P.; Nadjo, L.; Savéant, J.-M. *J. Electroanal. Chem.* **1973**, *42*, 223.
(12) The question of the dimerization mechanism is approached by careful measurement of changes in peak potential and shape with voltammetric scan rate. See papers in ref 11.
(13) (a) Pugh, J. R.; Meyer, T. J. *J. Am. Chem. Soc.* **1992**, *114*, 3785. (b) Watkins, W. C.; Jaeger, T.; Kidd, C. E.; Fortier, S.; Baird, M. C.; Kiss, G.; Roper, G. C.; Hoff, C. D. *J. Am. Chem. Soc.* **1992**, *114*, 907. (c) Tenhaff, S. C.; Covert, K. J.; Castellani, M. P.; Grunkenmeier, J.; Kunz, C.; Weakley, T. J. R.; Koenig, T.; Tyler, D. R. *Organometallics* **1993**, *12*, 5000. (d) Woska, D. C.; Ni, Y.; Wayland, B. B. *Inorg. Chem.* **1999**, *38*, 4135. (e) Hoff, C. D. *Coord. Chem. Rev.* **2000**, *206−207*, 451. (f) Miholva, D.; Vlcek, A. A. *Inorg. Chim. Acta* **1980**, *41*, 119. (g) Dessy, R. E.; Pohl, R. L.; King, R. B. *J. Am. Chem. Soc.* **1966**, *88*, 5121

A well-understood homoleptic metal carbonyl analogy involves the oxidation of $[Mn(CO)_5]^-$ to $Mn_2(CO)_{10}$.[15]

The fact that $E_{1/2}$(**2**) is *positive* of $E_{1/2}$(**1**) in the present case not only contrasts with previous literature but also appears to contradict the simple molecular-orbital model usually employed to account for redox-induced metal−metal dimerization processes.[16] We will show, however, that the solvation and ion-pairing effects of the medium play a more important role in these processes than previously recognized and, in the present case, tip the thermodynamic balance in favor of the dimer *radical*, allowing its direct voltammetric observation. Extension to the pentamethylcyclopentadienyl (Cp*) analogue $CoCp^*(CO)_2$, **3**, showed that it also undergoes R−S anodic coupling to give the corresponding dimer radical and, in a second anodic wave, $[Co_2Cp_2^*(CO)_4]^{2+}$. The Cp* radical dimer is less long-lived than $\mathbf{2}^+$ and undergoes a slow loss of CO. These findings offer a contribution to the emerging area of organometallic redox chemistry in low nucleophilicity media.[9,17]

Experimental Section

Experimental procedures were performed under nitrogen using either standard Schlenk conditions or a Vacuum Atmospheres drybox. Reagent-grade solvents were first distilled from appropriate drying agents into round-bottom storage flasks that contained CaH_2 (for dichloromethane, dichloroethane, and benzotrifluoride), potassium (for diethylether, hexane, and pentane), or potassium/benzophenone (THF). On the day of a redox experiment, an appropriate amount of solvent was transferred under a static vacuum to a flask that was then put into the drybox. Acetone was distilled from $CaSO_4$ and stored over 3 Å molecular sieves, 1,2-difluorobenzene was dried over alumina, and nitromethane was distilled from CaH_2. Glassware used for electrochemical experiments was cleaned by placing it in a No-Chromix (Godax Laboratories, Inc.) solution for at least 12 h, followed by copious rinsings by nanopure water and subsequent drying for at least 12 h in a 120 °C oven. The hot glassware was then loaded into the drybox antechamber and placed under a vacuum to cool just prior to the experiment. Ferrocene, decamethylferrocene, and $CoCp(CO)_2$, **1**, were purchased from Strem and used as received. $CoCp^*(CO)_2$, **3**, ($Cp^* = C_5Me_5$) was prepared according to the literature method,[18(a)] purified by sublimation (40 °C, 10^{-2} Torr), and checked by melting point (58 °C, sealed tube) and C, H analysis (Robertson Laboratories). The dinuclear complex $Co_2Cp_2^*(\mu\text{-}CO)_2$ was also prepared according to the literature method.[18b]

Electrochemistry. A standard three-electrode configuration was employed for voltammetry and electrolysis experiments. A PARC 273A potentiostat was employed in conjunction with homemade software linking the potentiostat to a personal computer. Excepting IR spectroelectrochemistry, electrochemical experiments were conducted inside a Vacuum Atmospheres Drybox under nitrogen. The drybox was outfitted with a cooling bath capable of controlling solution temperatures to better than 1 °C. Oxygen levels in the drybox were typically 1−5 ppm during the course of an experiment. Bulk electrolyses were carried out in an "H-type" cell having counter and working compartments separated by a fine glass frit. Most voltammetry scans were recorded using a glassy carbon working electrode disk of either 1.5 mm diameter (Cypress) or 1 or 2 mm (Bioanalytical Systems). The effective area of the 1 mm electrode was determined to be 8.1×10^{-3} cm^2 through a chronoamperometry experiment using ferrocene in acetonitrile/0.1 M $[NBu_4][PF_6]$. This value was used in digital simulations and for determination of diffusion coefficients of the analytes. The disks were pretreated using a standard sequence of polishing with diamond paste (Buehler) of decreasing sizes (3 μ to 0.25 μ), interspersed by washings with nanopure water, and final vacuum drying. The working electrode for bulk electrolyses was made of basket-shaped platinum gauze.

All potentials given in this paper are referred to the ferrocene/ferrocenium reference couple, as recommended elsewhere.[19] When decamethylferrocene was used as an internal standard, the experimentally measured potential was converted to the ferrocene potential by addition of −0.61 V, which is the $E_{1/2}$ of decamethylferrocene vs $FeCp_2^{0/+}$ measured in CH_2Cl_2/0.05 M $[NBu_4][B(C_6F_5)_4]$ in our laboratory.

Mechanistic aspects of redox processes were obtained from cyclic voltammetry (CV) data. Initially, diagnostic criteria involving shapes and scan rate responses of the CV curves were applied using procedures described elsewhere.[20] Later, digital simulations were performed using Digisim 3.0 (Bioanalytical Systems).

$[NBu_4][PF_6]$ was prepared by metathesis of $[NBu_4]I$ and $[NH_4][PF_6]$ in hot acetone, recrystallized several times from 95% ethanol, and vacuum-dried at 100 °C. Metathesis of $[NBu_4]Br$ with $M[B(C_6F_5)_4]$ (M = Li or K, Boulder Scientific) in aqueous methanol gave $[NBu_4][B(C_6F_5)_4]$, which was subsequently recrystallized from dichloromethane/ether. A detailed description has been published.[21] $[NBu_4][B(C_6H_3(CF_3)_2)_4]$ was prepared as follows. A solution of 3.86 g (12 mmol) of $[NBu_4]Br$ in 15 mL of a 2:1 methanol/water mixture was added dropwise to 10 g (11.3 mmol) of $Na[B(C_6H_3(CF_3)_2)_4]$ (Boulder Scientific) in a 30 mL 2:1 methanol/water mixture with stirring over a 15 min period. The resulting clear solution was then added dropwise to 300 mL of water over 1 h (faster additions may result in oils). The off-white precipitate was filtered off and air-dried. The crude material was purified by passing solutions of it through Brockman activity II alumina (typically, 2 g of the solid in 7 mL of methanol/5 mL of hexane through a 20 cm × 2.5 cm column, using approximately 400 mL of the same ratio methanol/hexane mixture). The solution was then added dropwise with vigorous stirring to 300 mL of water. The resulting precipitate was collected, air-dried, and then dried under a vacuum at 80 °C.

Spectroscopy. IR spectra were recorded with an ATI-Mattson Infinity Series FTIR interfaced to a computer employing Winfirst software at a resolution of 4 cm^{-1}. NMR spectra were recorded using a Bruker ARX 500 MHz spectrometer, and ESR spectra were obtained on a Bruker ESP 300E spectrometer. IR spectroelectrochemistry was performed using a mid-IR fiber-optic "dip" probe (Remspec, Inc), as described earlier,[22] with a standard H-type electrolysis cell operated under (argon) Schlenk conditions at 273 K. Bulk electrolysis was carried out with a Pt basket electrode, and the spectrum of the electrolysis solution was monitored as the electrolysis proceeded. At certain points (after, e.g., passage of half the number of expected coulombs of charge), the electrolysis was halted and voltammograms were recorded while the IR spectrum was being measured. This process generally required

(14) Fonseca, E.; Geiger, W. E.; Bitterwolf, T. E.; Rheingold, A. L. *Organometallics* **1988**, *7*, 567 and references therein. See: Einstein, F. W. B.; Jones, R. H.; Zhang, X.; Yan, X.; Nagelkerke, R.; Sutton, D. *J. Chem. Soc., Chem. Commum.* **1989**, 1424 for a non-electrochemical description of an Ir analogue.
(15) Kochi, J. K. In *Organometallic Radical Processes*; Trogler, W. C., Ed.; Elsevier: Amsterdam, 1990; pp 204−209.
(16) In a simple MO model, the interaction of two monomer orbital fragments creates a bonding, antibonding pair in the dimer. If three electrons are present, the energy of the dimer SOMO is higher than that of the original monomer orbital, making removal of an electron more facile from the former than from the latter (vide infra, Scheme 3).
(17) (a) Hill, M. G.; Lamanna, W. M.; Mann, K. R. *Inorg. Chem.* **1990**, *30*, 4687. (b) LeSuer, R. J.; Geiger, W. E. *Angew. Chem., Int. Ed.* **2000**, *39*, 248. (c) Barrière, F.; LeSuer, R. J.; Geiger, W. E. In *Trends in Molecular Electrochemistry*; Pombeiro, A. J. L., Amatore, C., Eds.; FontisMedia S. A.: Lausanne (Marcel Dekker Inc.: New York), 2004; pp 413−444.
(18) (a) Byers, L. R.; Dahl, L. F. *Inorg. Chem.* **1980**, *19*, 277. (b) Schore, N. E. *J. Organomet. Chem.* **1979**, *173*, 301.
(19) (a) Gritzner, G.; Kuta, J. *Pure Appl. Chem.* **1984**, *56*, 461. (b) Connelly, N. G.; Geiger, W. E. *Chem. Rev.* **1996**, *96*, 877.
(20) Geiger, W. E. In *Laboratory Methods in Electronalytical Chemistry*, 2nd ed.; Kissinger, P. T., Heineman, W. R., Eds.; Marcel Dekker, Inc.: New York, 1996; Chapter 23.
(21) LeSuer, R. J.; Buttolph, C.; Geiger, W. E. *Anal. Chem.* **2004**, *76*, 6395.
(22) Shaw, M. J.; Geiger, W. E. *Organometallics* **1996**, *15*, 13.

2 to 3 min, after which the electrolysis was continued to another stopping point until the electrolysis current was 1% or less of the original current.

DFT Calculations. All Density Functional Theory calculations[23] were performed using the Amsterdam Density Functional program package (ADF, versions 2004 and 2005).[24] Gradient corrected geometry optimizations[25] (gas phase and with solvent), without symmetry constraints, were performed using the Local Density Approximation of the correlation energy (Vosko−Wilk−Nusair),[26] augmented by the exchange-correlations funtionals of Perdew−Wang.[27] Relativistic effects were treated with the ZORA approximation.[28] The core orbitals were frozen for Co ($^{1-2}$s, 2p), Rh($^{1-3}$s,$^{2-3}$p, 3d), C, and O (1s). Triple-ζ Slater-type orbitals (STO) were used to describe the valence shells of C, O, H, and Co with a set of two polarization functions (p,f for Co and Rh; d,f for C,O; p,d for H). The solvent effects were included using the COnductor like Screening MOdel (COSMO)[29] implemented in ADF. The radius of the (rigid sphere) CH_2Cl_2 molecules was taken to be 2.449 Å.[30] To assign the radius of the solute, the van der Waals radii of the atoms were used (the atomic radius was taken in the case of cobalt): Co, 1.250 Å; C, 1.700 Å; O 1.520 Å; H 1.200 Å).[31] The dielectric constant of CH_2Cl_2 was 8.93.

For a given reaction $M \rightarrow M^+ + e^-$, the calculated adiabatic ionization potential $E(M^+) - E(M)$ (including structural relaxation) is the absolute oxidation potential (E). To compare the calculated values with the experimental ones, the correction for the Fc/Fc^+ reference absolute potential (4.98 eV) must be included.[32] The oxidation potential relative to the reference ($E_{ox}°$) was then calculated using $E_{ox}° = (\Delta G_{ox} - 4.98)/nF$, where n is the number of electrons and F is the Faraday constant.

Free energy changes (ΔG) for the $M \rightarrow M^+ + e^-$ reaction and the inclusion of the zero-point energy (ZPE) corrections should be considered in order to obtain better agreement between the calculated redox potentials and experimental ones, thus building an appropriate model for the redox reactions. The same applies for the calculation of dimerization energies. This requires, however, the computation of the vibrational frequencies, which is extremely demanding. On the other hand, Ziegler[33] has shown that the electrochemical behavior of cyclooctatetraene is mainly determined by electronic enthalpies. Therefore, we decided to follow this approach and calculate redox potentials based on electronic enthalpies, rather than free energies. The good agreement between calculated and experimental data proved this approximation to be valid. The dimerization energies were also computed based on electronic enthalpies, although the entropic contributions are expected to be relevant for an associative process.

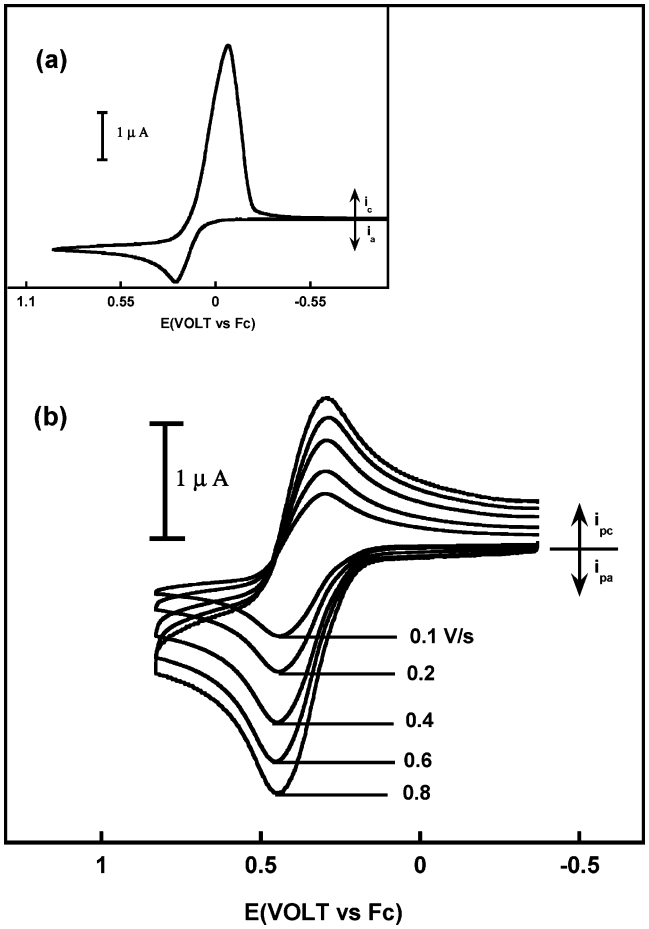

Figure 2. (a) Cyclic voltammogam of 2 mM **1** in CH_2Cl_2/0.1 M $[NBu_4][PF_6]$ at scan rate of 0.1 V/s, 298 K on a 1 mm GC disk. (b) Cyclic voltammogams of 0.25 mM **1** in CH_2Cl_2/0.05 M $[NBu_4][B(C_6F_5)_4]$ at different scan rates, 298 K on a 1 mm GC disk.

Results and Discussion

I. Electrochemical Oxidation of $CoCp(CO)_2$, 1. I.A. Anodic Behavior in Traditional Electrolyte Media. Previous investigations of the anodic oxidation of $CoCp(CO)_2$, **1**, have shown reversible CV behavior only at mercury electrodes, owing apparently to the formation of a mercury−cobalt complex on the electrode.[34,35] At solid electrodes the oxidation is patently irreversible in donor solvents such as acetonitrile. In nondonor lower-polarity solvents, such as dichloromethane, severe adsorption occurs because the positively charged oxidation product precipitates on the electrode as the salt of a traditional electrolyte anion.[34,36] The *inset* of Figure 2 gives an example of this adsorption behavior, which severely limits the electrochemical options. The much greater solubilities of salts of large weakly coordinating anions (WCAs) offer an antidote for anodic

(23) Parr, R. G.; Yang, W. *Density Functional Theory of Atoms and Molecules*; Oxford University Press: New York, 1989.
(24) (a) te Velde, G.; Bickelhaupt, F. M.; van Gisbergen, S. J. A.; Guerra, C. F.; Baerends, E. J.; Snijders, J. G.; Ziegler, T. *J. Comput. Chem.* **2001**, *22*, 931. (b) Guerra, C. F.; Snijders, J. G.; te Velde, G.; Baerends, E. J. *Theor. Chem. Acc.* **1998**, *99*, 391. (c) ADF2005.01, SCM, Theoretical Chemistry, Vrije Universiteit, Amsterdam, The Netherlands, http://www.scm.com.
(25) (a) Versluis, L.; Ziegler, T. *J. Chem. Phys.* **1988**, *88*, 322. (b) Fan, L.; Ziegler, T. J. *Chem. Phys.* **1991**, *95*, 7401.
(26) Vosko, S. H.; Wilk, L.; Nusair, M. *Can. J. Phys.* **1980**, *58*, 1200.
(27) Perdew, J. P.; Chevary, J. A.; Vosko, S. H.; Jackson, K. A.; Pederson, M. R.; Singh, D. J.; Fiolhais, C. *Phys. Rev.* **1992**, *B46*, 6671.
(28) van Lenthe, E.; Ehlers, A.; Baerends, E. J. *J. Chem. Phys.* **1999**, *110*, 8943.
(29) (a) Klamt, A.; Schüürmann, G. *J. Chem. Soc., Perkin Trans.* **1993**, *2*, 799. (b) Klamt, A. *J. Phys. Chem.* **1995**, *99*, 2224. (c) Klamt, A.; Jonas, V. *J. Chem. Phys.* **1996**, *105*, 9972. (c) Pye, C. C.; Ziegler, T. *Theor. Chem. Acc.* **1999**, *101*, 396.
(30) Reid, R. C.; Prausnitz, J. M.; Poling, B. E. *The Properties of Gases and Liquids*, 4th ed.; McGraw-Hill International, 1987; Appendix B, pp 733−734.
(31) Bondi, A. *J. Phys. Chem.* **1964**, *68*, 441.
(32) The value of 0.307 V vs SCE for Fc/Fc^+ was taken from Kuwana, T.; Bublitz, D. E.; Hoh, G. *J. Am. Chem. Soc.* **1960**, *82*, 5811. Then, this value is corrected with the well known potential of SCE vs SHE (0.241 V). The absolute Fc/Fc^+ potential is calculated adding to the previous value, 4.43 V, which is the absolute potential of SHE taken from Reiss, H.; Heller, A. *J. Phys. Chem.* **1985**, *89*, 4207.
(33) Baik, M.; Schauer, C. K.; Ziegler, T. *J. Am. Chem. Soc.* **2002**, *124*, 11167.
(34) This is well documented in Gennett, T.; Grzeszczyk, E.; Jefferson, A.; Sidur, K. M. *Inorg. Chem.* **1987**, *26*, 1856, who employed the medium CH_2Cl_2/$[NBu_4][PF_6]$. Reversible CV scans at a Hg electrode were briefly reported. The reversible redox couple is likely $2\ CoCp(CO)_2 + Hg \rightleftharpoons [Hg(Co_2Cp_2(CO)_4)]^{2+} + 2\ e^-$. At Pt or glassy carbon solid electrodes, chemically irreversible waves are observed if the solvent is acetonitrile and severe adsorption problems are encountered in dichloromethane if the supporting electrolyte anion is $[PF_6]^-$ (ref 35 and unpublished observations in our laboratory).
(35) Schore, N. E.; Ilenda, C. S.; Bergman, R. G. *J. Am. Chem. Soc.* **1977**, *99*, 1781.
(36) Similar cathodic stripping peaks are seen for **1** in CH_2Cl_2 containing $[PF_6]^-$ or $[BF_4]^-$, and similar results have been obtained in this laboratory for other piano-stool oxidations using the traditional anions.

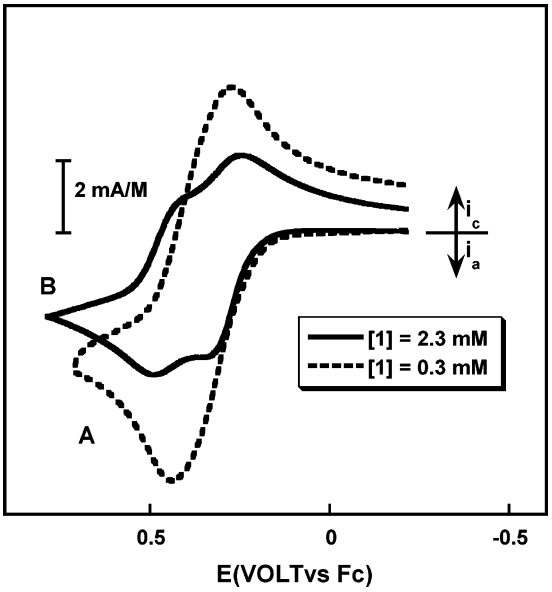

Figure 3. Cyclic voltammograms of **1** in CH_2Cl_2/ 0.05 M $[NBu_4][TFAB]$ at 298 K, on a 1 mm GC disk, and at a scan rate of 0.5 V/s at different concentrations; *y*-axis is concentration-normalized current.

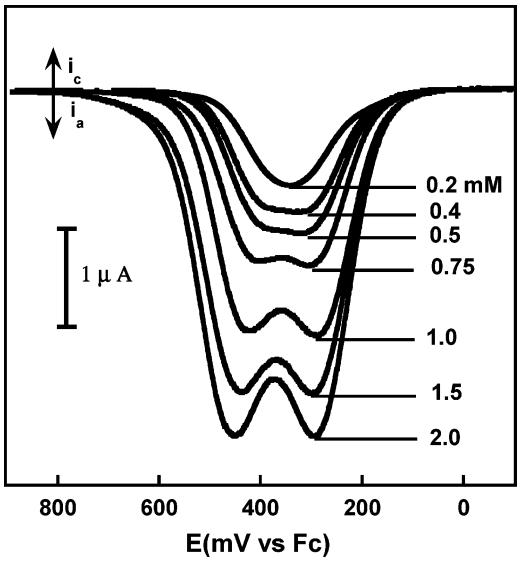

Figure 4. Square-wave voltammograms of **1** in CH_2Cl_2/ 0.05 M $[NBu_4]$-[TFAB] at different concentrations and at a frequency of 10 Hz, ambient temperature, at a 1 mm GC disk electrode.

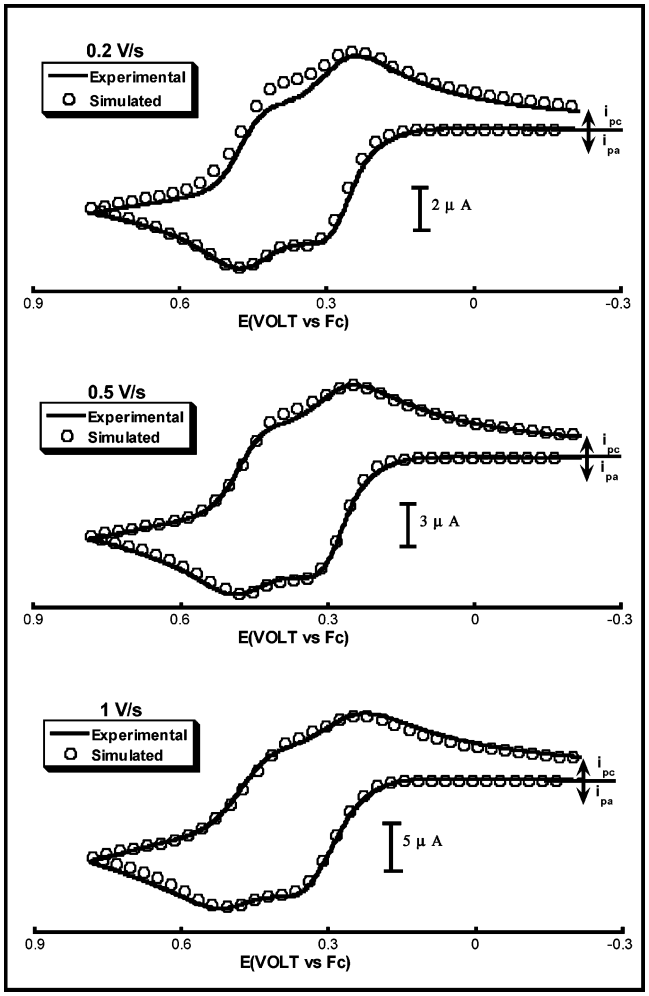

Figure 5. Experimental (solid curves) and simulated (circles) cyclic voltammograms of 2.27 mM **1** in CH_2Cl_2/0.1 M $[NBu_4][B(C_6F_5)_4]$ at different scan rates, 298 K and 1 mm GC disk electrode; simulation parameters are as follows: $E_{1/2}(1) = 0.37$ V, $\alpha_1 = 0.5$, $k_s^1 = 0.1$ cm/s, $E_{1/2}(2) = 0.47$ V, $\alpha_2 = 0.5$, $k_s^1 = 0.01$ cm/s, $K_{eq} = 3 \times 10^4$ M^{-1}, $k_{dim} = 4 \times 10^6$ M^{-1} s^{-1}. Consistent with the higher molecular weights of the dimers, their diffusion coefficients were set at lower values (1.12×10^{-5} cm^2 s^{-1}) than those of the monomers (2.32×10^{-5} cm^2 s^{-1}).

electrode adsorption in lower-polarity solvents.[37] Consequently, the oxidation of **1** was carried out in low-donor solvents using tetrabutylammonium salts of $[B(C_6F_5)_4]^-$ (TFAB) or $[B((C_6H_3(CF_3)_2)_4]^-$ ($BArF_{24}$) as supporting electrolytes.

I.B. Voltammetry of 1 in WCA Electrolytes. CV scans of **1** in CH_2Cl_2/$[NBu_4][TFAB]$ indicated clean electrode behavior in which, at least at fairly low concentrations (e.g., 0.25 mM **1**, Figure 2), an almost reversible-looking anodic wave was seen, with $E_{1/2}$ near 0.37 V, attributed to the couple $\mathbf{1}/\mathbf{1}^+$. Application of the usual diagnostic criteria[20] suggested, however, that $\mathbf{1}^+$ was subject to a follow-up reaction[38] and, at higher concentrations, a second anodic feature appeared at a potential close to the first. The concentration-normalized CVs of Figure 3 show contrasting shapes at the high and low concentrations of, respectively, 2.3 mM (solid line) and 0.3 mM (dashed line). The two features at high concentration, taken together, pass the current expected for a one-electron process.[39] This general picture emerges also with square-wave voltammograms (SWV), in which a single broad peak is seen at low concentrations and a resolved pair of equal height (with $E_{1/2}$ values of 0.37 and 0.47 V) is seen at high concentrations (Figure 4). Very similar concentration-dependent voltammetry was observed in other low-donor solvents.[40]

I.C. Oxidative Mechanism of 1. The anodic behavior of **1** obeys Scheme 1, which is a structural representation of the ECE

(37) (a) Camire, N.; Mueller-Westerhoff, U. T.; Geiger, W. E. *J. Organometal. Chem.* **2001**, *637*−*639*, 823. (b) Barrière, F.; Kirss, R. U.; Geiger, W. E. *Organometallics* **2005**, *24*, 48.

(38) For instance, at $\nu = 0.1$ V s^{-1} the ratio i_{rev}/i_{fwd} was only 0.83. The peak separation was also much larger (ca. 130 mV) than expected.

(39) This was quantitatively confirmed by chronocoulometry based on a diffusion coefficient of $(2.316 \pm 0.042) \times 10^{-5}$ cm^2/s. For a general description of the chronocoulometry method, see Bard, A. J.; Faulkner *Electrochemical Methods*, 2nd ed.; John Wiley & Sons, New York, 2001; pp 159 ff. Also relevant are steady-state voltammetry scans (1 mm glassy carbon electrode, 2 mV/s scan rate) of the two anodic waves. Their total combined current was equal to that observed for the cathodic wave at $E_{1/2} = -2.08$ V, $T = 273$ K arising from the one-electron reduction of **1**.

Scheme 1

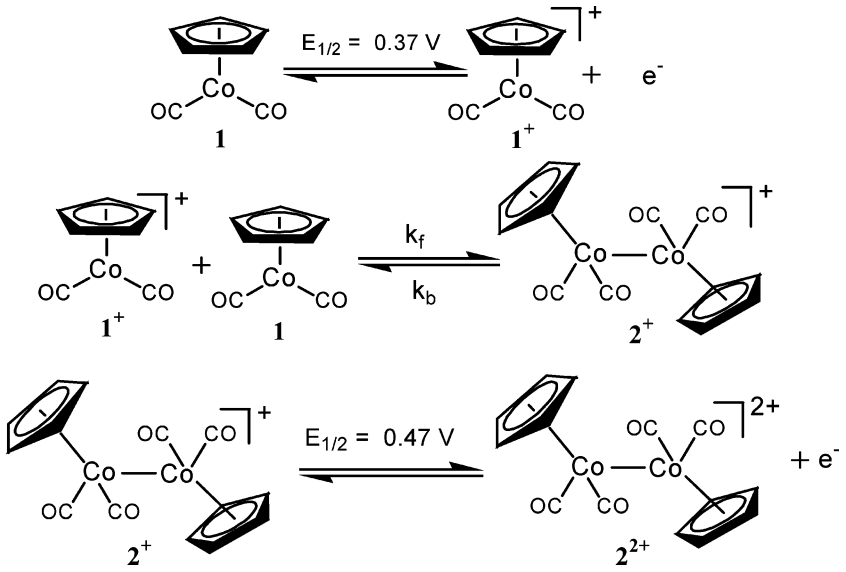

sequence of eqs 1−3. The key step in this mechanism is eq 2, the "C" reaction of the 17-electron radical $\mathbf{1}^+$ with the 18-electron complex **1** to give a metal−metal bonded dimer *mono*cation, $\mathbf{2}^+$, through a *radical−substrate* (R−S) coupling reaction. The dimer radical is subsequently oxidized to the corresponding dication, $\mathbf{2}^{2+}$, in the second wave at 0.47 V. This mechanism was confirmed by digital simulations of background-subtracted, iR-compensated, CV scans at a number of different concentrations and scan rates. The optimum simulation parameters, given in the caption of Figure 5, gave acceptable agreement with experiment. The fact that the experimental CV in this figure gave slightly less current on the reverse scan at the slowest scan rates may arise from edge-diffusion effects at the fairly small (1 mm diameter) electrode being employed.[41] The transfer coefficients (α values) were set at 0.5, consistent with the symmetric shapes of the waves. The heterogeneous electron-transfer rate constant ($k_s = 0.01$ cm s^{-1}) used for the redox pair $\mathbf{2}^+/\mathbf{2}^{2+}$ was somewhat lower than that of the $\mathbf{1}/\mathbf{1}^+$ couple, ($k_s = 0.1$ cm s^{-1}). Although the k_s values were not obtained with high precision, the difference in charge-transfer rates is qualitatively consistent with the fact that there is a major change in metal−metal bond distance for the $\mathbf{2}^+/\mathbf{2}^{2+}$ pair (vide infra). These simulations allowed quantitation of the fast and reversible radical−substrate reaction (of $\mathbf{1}^+$ with **1**) favoring $\mathbf{2}^+$ (eq 2, $K_{eq} = 3 \times 10^4$ M^{-1}; $k_f = 4 \times 10^6$ M^{-1} s^{-1}). The K_{eq} value shows that the 17-electron radical $\mathbf{1}^+$ will be present at very minor levels when it is generated in the presence of even modest concentrations of **1** (e.g., 11% when $\mathbf{1} = 2$ mM). Hence, as shown below, the dimer monocation $\mathbf{2}^+$ dominates in bulk electrolysis, IR, and ESR studies of the half-electron equivalent oxidation of **1**.

I.D. Bulk Electrolysis and IR Spectroscopy of Dimer Mono- and Dications. Exhaustive bulk oxidations of solutions containing 0.35 to 2 mM **1** in CH_2Cl_2/0.05 M [NBu_4][TFAB] at 298 K or 273 K and $E_{appl} = 0.7$ to 0.9 V (more positive than the second anodic wave) gave a sequential color change from the golden yellow of **1** to the green of $\mathbf{2}^+$ and finally to the light yellow of $\mathbf{2}^{2+}$ when electrolysis was complete (1.03 ± 0.06 F/equiv). A small amount of cobaltocenium ion was noted as a decomposition product ($E_{1/2} = -1.33$ V),[42] but back-electrolysis at $E_{appl} = -0.35$ V regenerated **1** in good yield.

IR spectra of the dimeric products were obtained through in situ spectroscopy (Figure 6) utilizing a fiber-optic probe.[22,43] As the electrolysis proceeded, the two bands for **1** (2023 and 1957 cm^{-1} in $C_2H_4Cl_2$) decreased in intensity and product peaks began to appear, first at 2090 cm^{-1} and 2040 cm^{-1} for $\mathbf{2}^+$, and then also at 2132 cm^{-1} and 2100 cm^{-1} for $\mathbf{2}^{2+}$ (Figure 6a, up to 0.5 F/equiv passed). Further electrolysis to completion (1 F/equiv, Figure 6b) confirmed the assignments, which are collected in Table 1.[44] It is important to note that, while not shown in Figure 6, spectra in the bridging carbonyl region were blank and *only terminal carbonyls are found* for the oxidation products of **1**. Comparison of the two most intense bands of the dimeric products with those of **1** reveals average increases in ν_{CO} energies of 75 cm^{-1} and 126 cm^{-1} for $\mathbf{2}^+$ and $\mathbf{2}^{2+}$, respectively. Based on considerable literature involving one-electron oxidations of mononuclear systems,[45] the 126 cm^{-1} shift is consistent with a full unit change in the metal oxidation

(40) There were subtle differences in the overall voltammetric behavior in other low-donor solvents. As expected, voltammetry in 1,2-dichloroethane was virtually identical to that observed in CH_2Cl_2. However, observable differences in wave positions and shapes occur in benzotrifluoride and in 1,2-difluorobenzene. Although these solvent effects may be commented on at a future time, it is important to note that they were all consistent with the proposed mechanism for the oxidation of **1**. A single chemically irreversible wave was observed in acetonitrile and THF, consistent with a nucleophilic attack of the donor solvent on $\mathbf{1}^+$.

(41) Longmire, M. L.; Watanabe, M.; Zhang, H.; Wooster, T. T.; Murray, R. W. *Anal. Chem.* **1990**, *62*, 747.

(42) The cobaltocenium/cobaltocene potential of −1.33 V vs ferrocene has been shown to be independent of the medium. See ref 19a. This assumption was confirmed in our laboratory for CH_2Cl_2/[NBu_4][TFAB].

(43) The dimer dication, $\mathbf{2}^{2+}$, was sufficiently stable to allow recording of its IR spectrum by transfer of an electrolysis sample to a conventional IR cell, followed by removal from the drybox. However, the in situ fiber-optic method offered a more quantitative approach.

(44) Inspection of the relative intensity changes for the two bands at 2023 cm^{-1} and 1957 cm^{-1} suggests that there is also a third feature for $\mathbf{2}^+$ at ca. 2023 cm^{-1}, overlapped with the higher energy band of **1**. This would be consistent with vibrational coupling of the two dicarbonyl moieties through a metal−metal bond and is included in the assigned ν_{CO} bands of $\mathbf{2}^+$. Based on a similar reasoning, we tentatively assign a third, weak feature at ca. 2040 cm^{-1} to $\mathbf{2}^{2+}$.

(45) (a) Nakamoto, K. *Infrared and Raman Spectra of Inorganic and Organometallic Compounds*, 4th ed.; John Wiley: New York, 1986; pp 291−295. (b) Goldman, A. S.; Krogh-Jespersen, K. *J. Am. Chem. Soc.* **1996**, *118*, 12159 (c) Willner, H.; Aubke, F. *Angew. Chem., Int. Ed.* **1997**, *36*, 2403.

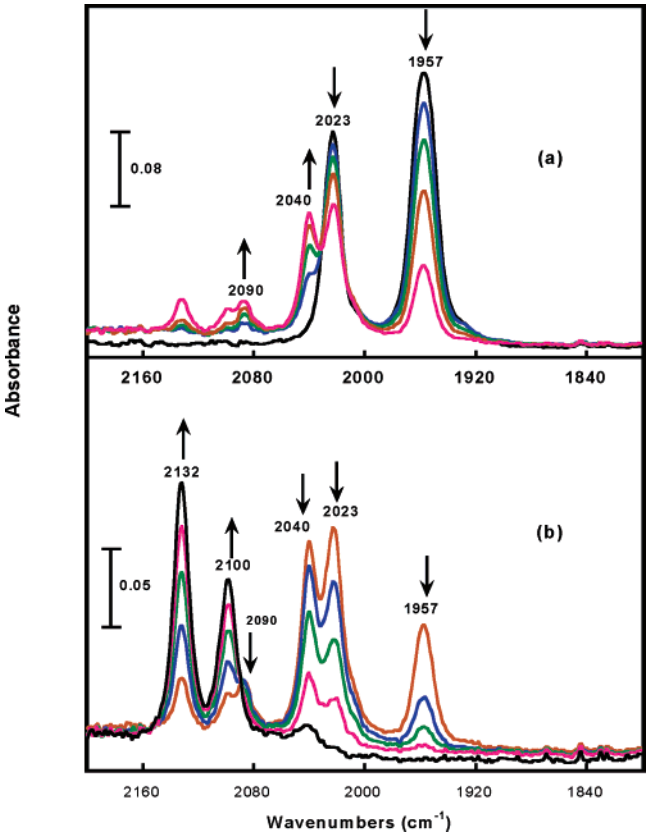

Figure 6. In situ IR spectroelectrochemistry of 2.7 mM **1** in $C_2H_4Cl_2$/0.05 $[NBu_4][BArF_{24}]$ recorded during bulk electrolysis at $E_{app} = 0.9$ V vs $Fc^{0/+}$ at 273 K (a) halfway electrolysis and (b) complete electrolysis.

Table 1. Redox Potentials of the Cobalt Systems Reported in This Work[a]

redox process	$E_{1/2}$ (V vs $FeCp_2^{0/+}$)
$[CoCp(CO)_2]^{0/+}$	0.37
$[Co_2Cp_2(CO)_4]^{+/2+}$	0.47
$[CoCp^*(CO)_2]^{0/+}$	−0.08
$[Co_2Cp^*_2(CO)_4]^{+/2+}$	0.05
$[Co_2Cp^*_2(\mu\text{-}CO)(CO)_2]^{+/0}$	−0.62
$[Co_2Cp^*_2(\mu\text{-}CO)_2]^{0/-}$	−2.0

[a] $E_{1/2}$ values are reported vs ferrocene in CH_2Cl_2/0.05 M $[NBu_4]$[TFAB], except for the oxidation products of **1**, which were measured in $C_2H_4Cl_2$/0.05 $[NBu_4][BArF_{24}]$.

state when going from **1** to $\mathbf{2}^{2+}$. While there seems to be no direct literature precedence for ν_{CO} shifts in the dinuclear *mono*cation, the measured shift of 75 cm^{-1} seems reasonable when compared to those of carbonyl-containing M−M bonded delocalized mixed-valent systems having bridging ligands, such as $[(Cr(CO)_2)_2(biphenyl)(\mu\text{-dppm})]^+$, for which an average shift of 60 cm^{-1} from the neutral complex has been reported.[46]

I.E. ESR Spectra of Dimer Radical Cation $\mathbf{2}^+$. Samples of a light green solution containing $\mathbf{2}^+$, generated through a 0.5 F/equiv electrolysis of 2 mM **1** in CH_2Cl_2/0.05 M $[NBu_4]$[TFAB], showed intense ESR activity. The fluid solution spectra ($g_{iso} = 2.0373$) had broad lines, but resolution of the middle hyperfine components was observed at 273 K (Figure 7a). Variable and asymmetric broadening of the various hyperfine components arises from the well-understood dependence of relaxation rate on the m_I component of each line.[47] With

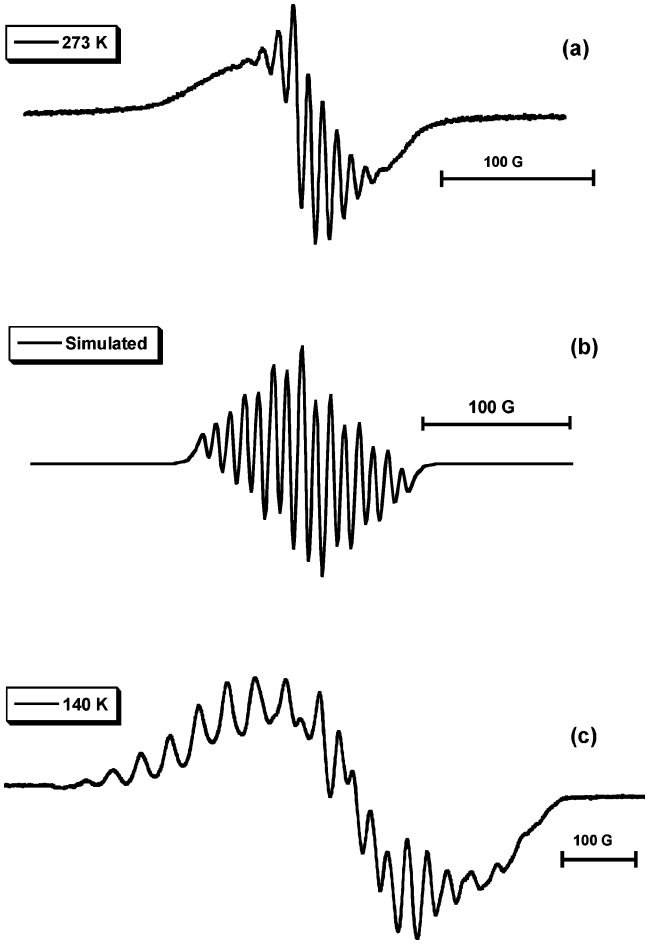

Figure 7. (a) ESR fluid spectrum (recorded at 273 K, microwave power = 15.9 mW, modulation amplitude = 5 G) of the electrochemically generated dimer monocation, $[Co_2Cp_2(CO)_4]^+$ in CH_2Cl_2/0.05 M $[NBu_4]$-[TFAB] at $E_{app} = 0.9$ V, 273 K. (b) Simulated ESR spectrum, line width = 5 G; $\langle a \rangle = 10$ G; $g = 2.0273$ G (c) ESR frozen spectrum of the dimer monocation recorded at 140 K.

observation of as many as 10 of the expected 15 hyperfine lines for interaction with two equivalent ^{59}Co nuclei ($I = 7/2$), an isotropic hyperfine splitting, $\langle a_{Co} \rangle$, of 10 G was assigned and confirmed by simulation (Figure 7b) agreeing with the middle part of the fluid spectrum. A strong frozen-solution spectrum (140 K) was also observed. The principal hyperfine feature (Figure 7c) is a 15-line pattern with a splitting of $A_1(Co) = 40$ G. Unresolved features arising from smaller cobalt splittings are also seen in the middle of the spectrum. If one assumes an axial or nearly axial spectrum, the measured values of $A_1(Co)$ and $\langle a_{Co} \rangle$ can be used to estimate the % Co d-orbital character in the SOMO through calculation of the "uniaxial hyperfine splitting value" (B).[48] In the present case, this analysis is hampered not only by the unverified assumption of axial symmetry but also by the fact that the relative signs of $A_1(Co)$ and $\langle a_{Co} \rangle$ are unknown. Nevertheless, it can be shown that if the signs of $A_1(Co)$ and $\langle a_{Co} \rangle$ are the same, then $B = 15.5$ G. If they are different, $B = 25$ G. Both values are small compared to the theoretical value of $B_o = 120$ G expected for an orbital having purely Co d-character.[48b] The larger of the two values,

(46) Atwood, C. G.; Geiger, W. E. *J. Am. Chem. Soc.* **2000**, *122*, 5477.

(47) Carrington, A.; McLachlan, A. D. *Introduction to Magnetic Resonance*; Harper & Row: New York, 1967, pp 197−199.

(48) (a) Weil, J. A.; Bolton, J. R.; Wertz, J. E. *Electron Paramagnetic Resonance*; Wiley & Sons, New York, 1984; p 116 (b) Ibid.; p 534.

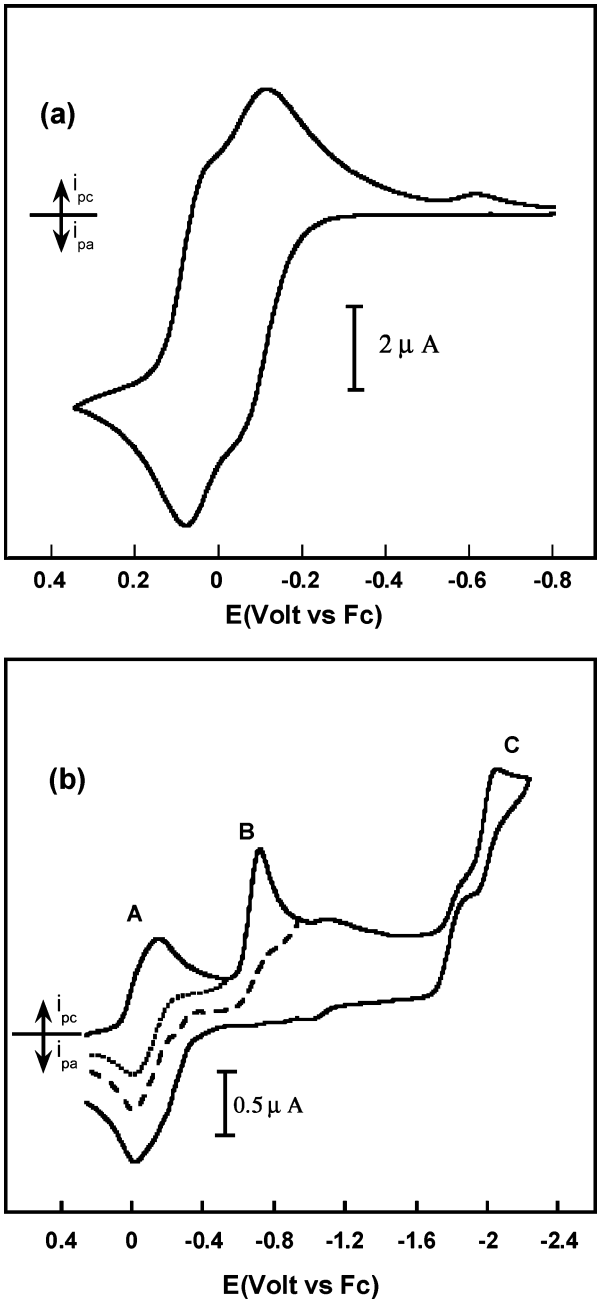

Figure 8. (a) Cyclic voltammogams of 4 mM **3** in CH_2Cl_2/0.05 M $[NBu_4][B(C_6F_5)_4]$ at a scan rate of 0.1 V/s, 298 K on a 1 mm GC disk. (b) CVs recorded after halfway bulk electrolysis of 0.75 mM **3** in CH_2Cl_2/0.05 M $[NBu_4][B(C_6F_5)_4]$ at 298 K, $E_{appl} = 0.3$ V, scan rate = 0.2 V/s, and a 1 mm GC disk electrode.

coming from the more likely case of different signs for A_1(Co) and $\langle a_{Co} \rangle$, places about 20% spin on each Co atom in the SOMO of $\mathbf{2}^+$, with the remainder of the spin being delocalized into the ligands. DFT calculations predict about twice this amount of metal character for the SOMO (vide infra). Accounting for the quantitative inequality of the ESR and DFT spin-density results would require more experimental data, possibly involving Q-band measurements for better delineation of the Co hyperfine spittings.

It is interesting that the cobalt contribution to the SOMO of $\mathbf{2}^+$ is qualitatively similar to that observed for the carbonyl-bridged dicobalt *anion* $[Co_2Cp_2(\mu\text{-}CO)_2]^-$.[49] The latter is isoelectronic with $\mathbf{2}^+$ if a bond order of 1.5 is assigned to its metal−metal bond, and both systems have the unpaired electron in a Co−Co antibonding orbital.[50] Removal of that electron from $[Co_2Cp_2(\mu\text{-}CO)_2]^-$ gives a relatively small shortening of the Co−Co bond for the carbonyl-bridged system, as well demonstrated for the Cp* analogues {d_{Co-Co} 2.372 Å in $[Co_2Cp^*_2(\mu\text{-}CO)_2]^-$, 2.338 Å in $Co_2Cp^*_2(\mu\text{-}CO)_2$}.[50] By way of contrast, removal of the unpaired electron from $\mathbf{2}^+$, which lacks bridging carbonyls, dramatically shortens the Co−Co bond length from 3.14 Å for $\mathbf{2}^+$ to 2.64 Å for $\mathbf{2}^{2+}$ (vide infra).

II.A. Anodic Behavior of $CoCp^*(CO)_2$, 3. Gennett and coworkers have shown that $CoCp^*(CO)_2$, **3**, displays a single quasi-Nernstian one-electron oxidation in CH_2Cl_2/0.1 M $[NBu_4][PF_6]$ and that the 17-electron radical $\mathbf{3}^+$ is persistent after bulk oxidation of **3** at 253 K.[34] A contrasting CV behavior is found when the $[PF_6]^-$ anion is replaced by $[TFAB]^-$, namely two closely spaced waves which are reminiscent of the CV behavior of **1** under the same conditions (Figure 8a), except that the waves are more negative potentials ($E_{1/2}(1) = -0.08$ V, $E_{1/2}(2) = 0.05$ V), consistent with the electronic effect of permethylation of the Cp ring. Another small, irreversible, cathodic wave arising from a slower follow-up reaction is also observed (E_{pc} near −0.7 V). Like **1**, the anodic behavior of **3** was sensitive to scan rate, temperature, and concentration. Regarding the last of these, an essentially Nerstian single CV wave was seen at a low concentration (0.2 mM). In short, the CV behavior of **3** in $[TFAB]^-$-containing media mimicked that of **1**, suggesting the occurrence of a radical/substrate dimerization reaction between $\mathbf{3}^+$ and **3** to form the dimer radical $[Co_2Cp^*_2(CO)_4]^+$, $\mathbf{4}^+$ (eq 4), which is subsequently oxidized at 0.05 V to the dication $\mathbf{4}^{2+}$:

$$\underset{\mathbf{3}^+}{[CoCp^*(CO)_2]^+} + \underset{\mathbf{3}}{CoCp^*(CO)_2} \rightleftharpoons \underset{\mathbf{4}^+}{[Co_2Cp^*_2(CO)_4]^+} \quad (4)$$

The long-term anodic decomposition products are different, however, for **3**. In a number of bulk oxidations at different temperatures (243 to 298 K) and concentrations (0.16 mM to 3 mM), exhaustive electrolyses released 0.65 ± 0.06 F/equiv and gave several electrolysis products, as illustrated in Figure 8b. In this CV, taken *before* completion of the electrolysis,[51] wave A arises from the reduction(s) of the primary products $\mathbf{4}^{2+}$, $\mathbf{4}^+$, and $\mathbf{3}^+$. Waves B and C became more prominent at longer times and were chemically reversible at higher scan rates. Note that since wave C is negative of wave B, the former may either be present in the bulk of solution *or* be the product of the reduction wave B. With the help of IR spectroelectrochemistry (vide infra), the follow-up products were identified as the singly carbonyl-bridged dinuclear complex $[Co_2Cp^*_2(\mu\text{-}CO)(CO)_2]^+$, $\mathbf{5}^+$ (wave B, $E_{1/2} = -0.62$ V) and the doubly carbonyl-bridged complex $Co_2Cp^*_2(\mu\text{-}CO)_2$, **6** (wave C, $E_{1/2} = -2.0$ V).

(49) (a) Schore, N. E.; Ilenda, C. S.; Bergman, R. G. *J. Am. Chem. Soc.* **1977**, *99*, 1781. (b) ESR reported in Schore, N. E. *J. Organometal. Chem.* **1979**, *173*, 301. The assignment of the SOMO as being ca. 60% dimetal in nature was later questioned (Dudeney, N.; Green, J. C.; Kirchner, O. N.; Smallwood, F. St. J. *J. Chem. Soc., Dalton Trans.* **1984**, 1883) after photoelectron spectroscopy results suggesting bridging-ligand delocalized bonding in $Co_2Cp^*_2(\mu\text{-}CO)_2$. Discussions of structure and bonding in these bridged dimers may be found in these references and in ref 50.

(50) (a) Ginsberg, R. E.; Cirjak, L. M.; Dahl, L. F. *J. Chem. Soc., Chem. Commun.* **1979**, 468. (b) Bailey, W. I., Jr.; Collins, D. M.; Cotton, F. A.; Baldwin, J. C.; Kaska, W. C. *J. Organometal. Chem.* **1979**, *165*, 373. (c) Cirjak, L. M.; Ginsberg, R. E.; Dahl, L. F. *Inorg. Chem.* **1982**, *21*, 940.

(51) Figure 8 was recorded after 55% completion of electrolysis, based on number of Faradays passed compared to the number required for the electrolysis current to be 1% of original.

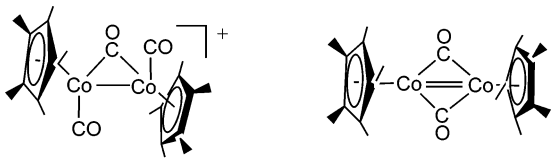

5^+ 6

II.B. IR Spectroelectrochemistry of $CoCp^*(CO)_2$. IR spectra recorded during electrolysis of **3** gave significant insight into the ultimate anodic fate of this compound on the synthetic time scale. Direct syringe sampling was compared with the in situ method in order to broaden the range of measurement conditions. Spectra obtained by the syringe-sampling method are given in the Supporting Information as Figure S1, and representative in situ spectra are shown in Figure 9. The cogent results are the following: (i) The disappearance of the bands at 1999 cm^{-1} and 1933 cm^{-1} for **3** accompanies the original oxidation, with the appearance of features at 2057 cm^{-1} and 1847 cm^{-1} along with weaker bands at 2107 cm^{-1} and 2069 cm^{-1} (the latter pair is shown in Figure S1 rather than in Figure 9). (ii) When the solution was bulk rereduced, but at a potential *insufficient* to reduce the product responsible for wave B of

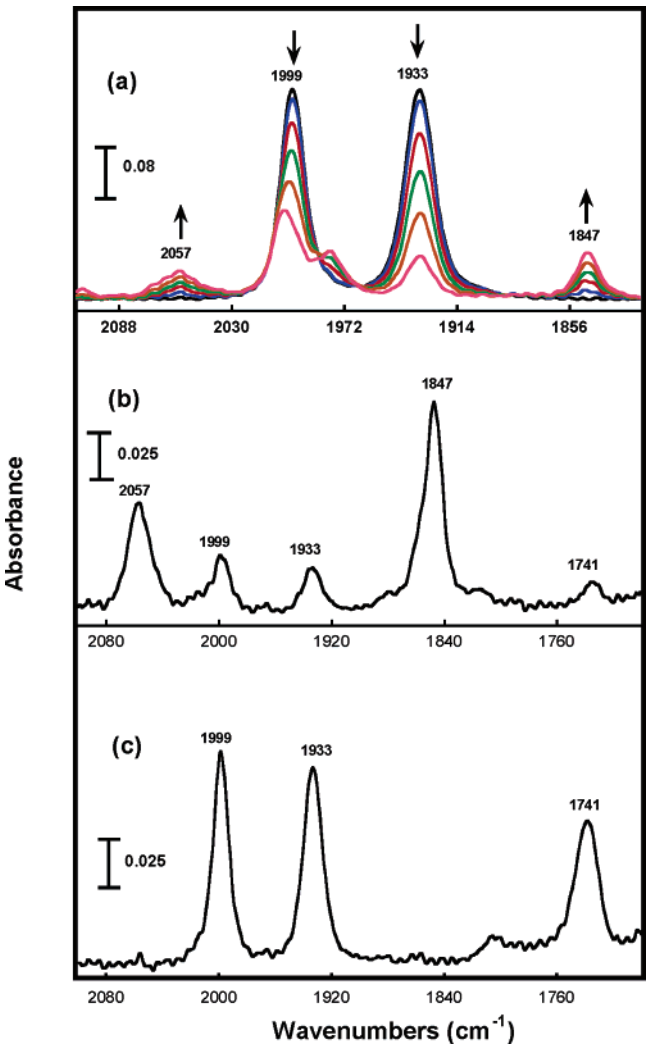

Figure 9. (a) In situ IR spectroelectrochemistry recorded during the first halfway bulk electrolysis of 2.6 mM **3** in CH_2Cl_2/0.05 M $[NBu_4][B(C_6F_5)_4]$. (b) IR spectra obtained after back reduction at wave A and (c) IR spectra recorded after back reduction at wave B.

Table 2. Carbonyl Region IR Bands Obtained during the Bulk Oxidation of **1**, **2** in DCE and DCM Containing 0.05 M $[NBu_4][TFAB]$, Respectively, and Calculated (DFT)

species	ν(CO) cm^{-1} (expt)	ν(CO) cm^{-1} (calcd)
$[CoCp(CO)_2]$	2023, 1957	2023,1972
$[Co_2Cp_2(CO)_4]^+$	2090, 2040, 2023	2012,2023,2028,2058
$[Co_2Cp_2(CO)_4]^{2+}$	2132, 2100, 2040	2108, 2085, 2078, 2069
$[CoCp^*(CO)_2]$	1999, 1934	
$[Co_2Cp^*_2(\mu\text{-CO})(CO)_2]^+$	2057, 1847	
$[Co_2Cp^*_2(CO)_4]^{2+}$	2107, 2069	
$[Co_2Cp^*_2(\mu\text{-CO})_2]$	1741	-

Scheme 2

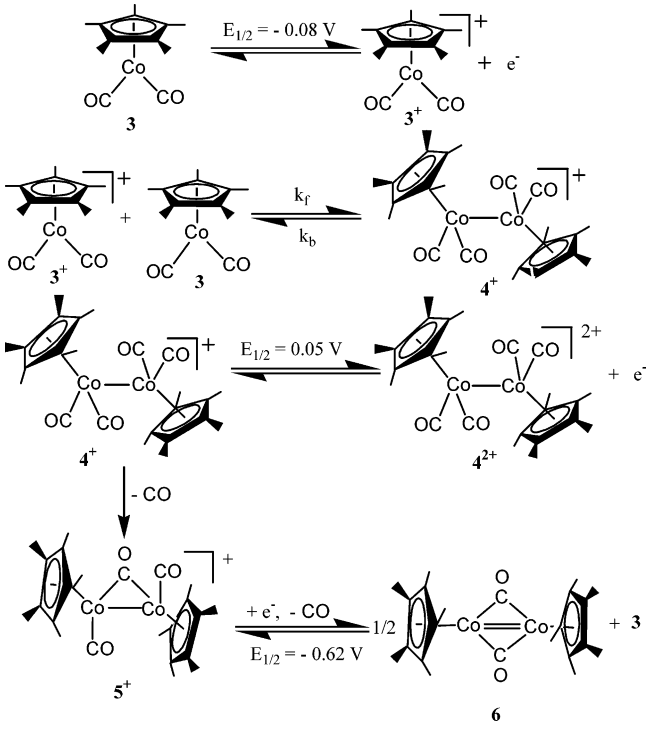

Figure 8b, the bands of neutral **3** reappeared as the pair at 2107 cm^{-1} and 2069 cm^{-1} disappeared, suggesting assignment of the latter pair to the primary dimer dication $\mathbf{4}^{2+}$. Given the electronic effect accompanying the replacement of Cp by Cp*, this assignment is consistent with the assignment of the ν_{CO} frequencies of $\mathbf{2}^{2+}$ (see Table 2). The major product waves at this point (Figure 9b, 2057 cm^{-1} and 1847 cm^{-1}) are attributed to the terminal and bridging carbonyls, respectively, of $[Co_2Cp^*_2(\mu\text{-CO})(CO)_2]^+$, $\mathbf{5}^+$. (iii) When the electrolysis was continued at a potential sufficient to reduce wave B, the only three bands of meaningful intensity (Figure 9c) were readily attributed to the starting material **3** and the doubly CO bridging compound $Co_2Cp^*_2(\mu\text{-CO})_2$, **6**, $\nu_{CO} = 1741$ cm^{-1}.

The conclusion that one-electron reduction of $\mathbf{5}^+$ ($E_{1/2} = -0.62$ V) results in formation of **3** and **6** is consistent with CV scans of the original anodic electrolysis solution (Figure 8b), in which a negative-going scan through wave B gave wave C, for which the $E_{1/2}$ value is known[18b] and confirmed by us under the present electrolyte conditions. Hence the long-term behavior of dimeric forms of oxidized **3** is shown to result in a slow loss of CO and formation of compounds having bridging CO groups. The overall process is shown in Scheme 2.

III.A. Bonding and Structures. DFT calculations were performed on complexes **1**, $\mathbf{1}^+$, $\mathbf{2}^+$, and $\mathbf{2}^{2+}$ both in the gas

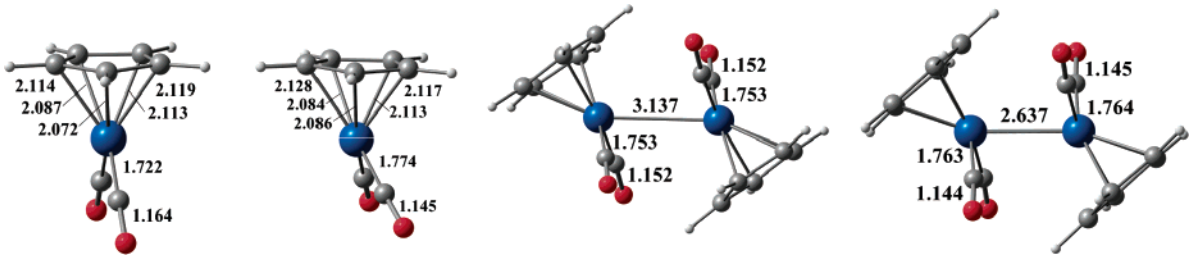

Figure 10. Optimized geometries (COSMO) of **1** (left), $\mathbf{1}^+$, (left center), $\mathbf{2}^+$ (right center), and $\mathbf{2}^{2+}$ (right).

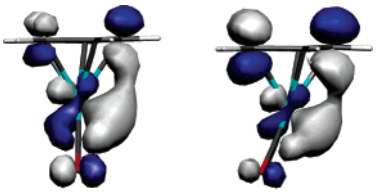

Figure 11. HOMO of $CoCp(CO)_2$ (**1**, left) and SOMO of $[CoCp(CO)_2]^+$ ($\mathbf{1}^+$, right) from the COSMO calculation.

phase and including solvent (COSMO model), in order to understand the nature of the formation of dimer $\mathbf{2}^+$ and its redox behavior. Although the geometries did not significantly change when the optimization procedure was carried out in the presence of the solvent, the energies varied significantly. Therefore, the discussion will address the results obtained from calculations with solvent, unless otherwise stated. The geometries of the four complexes are displayed in Figure 10, with some relevant distances. A complete set of structural parameters is given in Table S1 (gas-phase and solvent). For the dimers $\mathbf{2}^+$ and $\mathbf{2}^{2+}$, we report only the results for the most stable trans form, as similar results have been described for the conceptually related $ReCp(CO)_3$ system.[52]

An important structural parameter is the τ angle, defined as the angle between the centroid of the Cp ring, cobalt, and the midpoint of C(O)−C(O), which is associated with the C−Co−C angle. The largest change introduced by solvent effects was observed in the Co−C(O) distances and the τ angle of the $[CoCp(CO)_2]^+$ ($\mathbf{1}^+$) cation, which lengthened from 1.774 to 1.793 Å and narrowed from 160° to 157°, respectively (see Table S1). All the other differences were much smaller, indicating a negligible effect of solvent on the geometry.

In complex **1**, the OC−Co−CO angle is 93° and τ is 178°. Upon oxidation to the radical $\mathbf{1}^+$, the OC−Co−CO angle opens up to 98° (see Figure 10) and τ drops to 157°. The HOMO of **1** and the SOMO of $\mathbf{1}^+$ are shown in Figure 11.

The occupied orbital of the radical cation $\mathbf{1}^+$ resembles that found for the analogous radical $[ReCp(CO)_3]^+$.[52] Pyramidalization around the metal in both 17-electron systems results in the rehybridization of the metal orbitals toward the empty position, favoring interaction with another ligand[53] or metal center. Whereas this hybridization effect is not seen in the 18-electron Re analogue, it is already present, albeit to a smaller extent, in the HOMO of **1**, thereby facilitating the interaction between $\mathbf{1}^+$ and **1** and allowing formation of the R−S coupling product $\mathbf{2}^+$. By way of contrast, the neutral Re complex lacks the hybridized HOMO which would allow R−S coupling with $[CpRe(CO)_3]^+$, and dimerization to form $[Re_2Cp_2(CO)_6]^{2+}$ occurs through a radical−radical (R−R) mechanism.[52]

Scheme 3

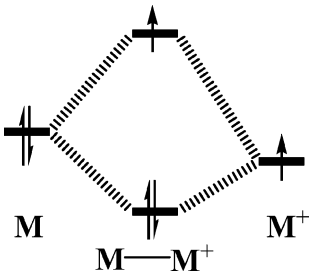

Scheme 3 is the simple MO picture that has traditionally represented interactions of the highest occupied orbitals of systems undergoing direct metal−metal bond formation. This three-electron model, in which the SOMO is found at relatively high energy, provides the rationale for the fact that removal of an electron from $M-M^+$ is *usually* more facile than electron removal from M. Thus, the dimer radical is usually thermodynamically *dis*favored, with a single anodic wave being observed for the oxidation of M to the dimer dication $[M-M]^{2+}$. The unique stability of the dicobalt radical cations is not explained by this simple two-orbital model, and a more in-depth treatment of the overall energies of these systems is given below (section III.B).

The fact that the SOMO is metal−metal antibonding does account, however, for the relationship between the computed Co−Co distances and the redox states of the dimer. Indeed, the long Co−Co distance in $\mathbf{2}^+$ (3.137 Å) shortens upon oxidation to $\mathbf{2}^{2+}$ (2.637 Å), reflecting the removal of one electron from the Co−Co σ^* SOMO orbital (Figure 12). The other relevant structural change of the dimer concerns the τ angle, which becomes 159° in each half of $\mathbf{2}^+$ (the dimers are essentially symmetric, despite the absence of symmetry constraints in the calculation) and drops significantly to 149° in each half of $\mathbf{2}^{2+}$, in order to adapt to the proximity of the Cp ring to the carbonyls.

III.B. Spectroscopic Parameters. Frequency calculations were carried out only in the gas phase in order to obtain the C═O stretching frequencies and compare them with experimental values. The results, without any scaling, are collected in Table 2. The agreement is almost perfect for the neutral complex **1** and quite acceptable for the charged dimers, where,

(52) Chong, D.; Nafady, A.; Costa, P. J.; Calhorda, M. J.; Geiger, W. E. *J. Am. Chem. Soc.* **2005**, *127*, 15676.

(53) The anodic oxidations of $Rh(\eta^5\text{-}C_5R_5)(CO)_2$, R = H or Me, have not been studied in detail in WCA-electrolyte solutions. In unpublished work, we observed a single anodic wave for $RhCp^*(CO)_2$ in CH_2Cl_2/0.1 M $[NBu_4]$-[TFAB], making it likely that any R−S intermediate is thermodynamically unstable in this system. If so, the oxidation would be proceeding directly from $RhCp^*(CO)_2$ to $[Rh_2Cp^*_2(CO)_4]^{2+}$, without detection of a dimer radical. Our calculations indicate a Rh−Rh bond length of 3.252 Å in $[Rh_2Cp_2(CO)_4]^+$ and 2.824 Å in $[Rh_2Cp_2(CO)_4]^{2+}$.

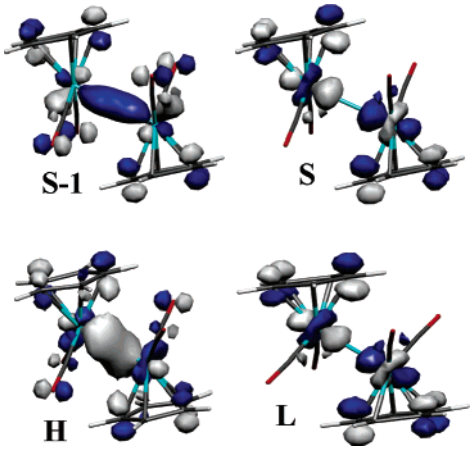

Figure 12. Frontier orbitals of the monocation $[\{CoCp(CO)_2\}_2]^+$ ($\mathbf{2}^+$, top, SOMO−1 and SOMO) and of the dication $[\{CoCp(CO)_2\}_2]^{2+}$ ($\mathbf{2}^{2+}$, bottom, HOMO and LUMO) from the COSMO calculation.

as mentioned earlier, the geometry changes a bit more when solvent effects are considered. Still, these values support the experimental assignment of the two species $\mathbf{2}^+$ and $\mathbf{2}^{2+}$.

The calculated spin density of the $\mathbf{2}^+$ radical cation is mostly located in the two cobalt atoms (about 40% in each), with smaller contributions from three carbon atoms of each Cp ring (8%, 4%, 4% per ring), in conceptual but not quantitative agreement with the ESR data (vide ante).

In all these species, the solvent effect is reflected in the solvation energy, which is very small for the neutral complex $CoCp(CO)_2$ (**1**, −7.5 kcal mol^{-1}), increases to −58.0 in $\mathbf{1}^+$, drops slightly in $\mathbf{2}^+$ as the same total charge of $\mathbf{1}^+$ becomes distributed in the larger cation, and reaches the maximum in $\mathbf{2}^{2+}$. Solvation effects are considered more broadly in section III.C.

III.C. Stability of the Dimer Radical. As pointed out above, the simple MO model of Scheme 3 fails to account for the anomalous stability of the dicobalt radical dimer $\mathbf{2}^+$. Therefore, the energies of the reactions for the cobalt/dicobalt system were calculated, and the results were contrasted with those of the rhodium/dirhodium analogue. The latter is known to display the traditional CV of a single anodic process going from neutral $RhCp(CO)_2$ to the dication $[Rh_2Cp_2(CO)_4]^{2+}$, the dimer radical being thermodynamically unstable.[53] The redox potentials for all the species, as well as the dimerization energies (see Experimental Section for details), are collected in Table 3. The first important outcome is that the experimental data available, namely $E°_1$ for Co and Rh, $E°_2$ for Co, and ΔH_f ($\mathbf{2}^+$), agree with the calculated values obtained from the COSMO calculation. Notice, as well, that the gas-phase numbers in parentheses are quite poor for both $CoCp(CO)_2$ and $RhCp(CO)_2$, showing the strong influence of the solvent effect. These trends are as expected when comparing energies of species with different charges.[54]

Interestingly, the gas-phase model predicts a highly favored dimerization energy for the Co system (−27.0 kcal mol^{-1}),

Table 3. Calculated (DFT, COSMO Model) Absolute and Relative to the Fc/Fc^+ Reference Redox Potentials E_n and $E°_n$ (V) for the Pairs $\mathbf{1}/\mathbf{1}^+$ and $\mathbf{2}^+/\mathbf{2}^{2+}$, Experimental $E°_n$ (Bold), and Dimerization Enthalpies ΔH_f (kcal mol^{-1})

	$\mathbf{1}/\mathbf{1}^+$		$(\mathbf{1}+\mathbf{1}^+ \rightarrow \mathbf{2}^+)$	$(\mathbf{1}^+ + \mathbf{1}^+ \rightarrow \mathbf{2}^{2+})$	$\mathbf{2}^+/\mathbf{2}^{2+}$	
	E_1	$E°_1$	$\Delta H_f(\mathbf{2}^+)$	$\Delta H_f(\mathbf{2}^{2+})$	E_2	$E°_2$
$CoCp(CO)_2$	5.38 (7.50)[a]	0.40 (2.52) **0.37**[b]	−11.6 (−27.0) **−6.1**[c]	−8.2	5.53 (10.24)	0.55 (5.26) **0.47**[b]
$RhCp(CO)_2$	5.35	0.37	−10.05	−16.36	5.07	0.09

[a] Gas-phase values. [b] This work. [c] Free energy estimated from $K_{eq} = 3 \times 10^4$ M^{-1}.

which is clearly overestimated. A more realistic value of −11.6 kcal mol^{-1} is obtained from the solvent model COSMO calculation which agrees more closely with the estimated experimental free energy calculated from K_{eq} (−6.1 kcal mol^{-1}), especially if we include the entropic term associated with an associative process ($\Delta S < 0$). The COSMO calculated values are in excellent agreement with the experimental values, reproducing the fact that $E°_2$ is more positive than $E°_1$ for the Co system but not for the Rh system. This means that the second oxidation of $\mathbf{2}^+$ must be more difficult than the oxidation of **1**, thereby having a more positive $E_{1/2}$ value, as observed.

Two main effects must be analyzed in order to understand the effect of the solvent on the oxidation potentials, namely the solvation energy and the structural relaxation derived from the presence of the solvent. In order to understand the origin of the global effect, an energy-partitioning scheme was considered.[33] Three contributions can be extracted: (i) the semiadiabatic ionization potential, (ii) the structural relaxation due to the removal of electrons, and (iii) the solvation energy. Ion-pairing effects were not taken into account.

Two energy-partition diagrams (gas phase and COSMO) are shown in Figure 13 for the oxidations of **1** and $\mathbf{2}^+$, with the lower portion being the calculations for the analogous Rh systems. Starting from the upper left corner, for Co, the diagonal (path I) goes from **1** to $\mathbf{1}^+$ ($E°_1$). The same path can be undertaken by removing one electron from **1** without allowing the structure to relax (single-point calculation, with structure of **1** and one electron less) to give $\mathbf{1}_{ox}^+$ (path Ia) and then relaxing the structure to $\mathbf{1}^+$ (path Ib), or by calculating the energy of **1** with the structure of $\mathbf{1}^+$ (path Ic) leading to $\mathbf{1}_s$ and then to $\mathbf{1}^+$ (path Id). The same was carried out for $\mathbf{2}^+$.

In the absence of relaxation ($\mathbf{1} \rightarrow \mathbf{1}_{ox}^+$), the removal of electrons is already easier in **1** than in $\mathbf{2}^+$, both in gas-phase and COSMO calculations. The removal of an electron from $\mathbf{2}^+$ is highly unfavorable in the gas phase. Inclusion of solvent effects lowers the oxidation potentials, especially of $\mathbf{2}^+$, making the semiadiabatic ionization potentials of **1** and $\mathbf{2}^+$ comparable. In the gas phase, the structural relaxation of **1** ($\mathbf{1} \rightarrow \mathbf{1}_s$) is smaller than that of $\mathbf{2}^+$ ($\mathbf{2}^+ \rightarrow \mathbf{2}^+_s$), but the order is reversed in the solvated model (steps **Ib** and **IIb**). The energies are comparable (−0.50 and −0.43, respectively) and are related, in **1**, to the change on the angle τ, and, in $\mathbf{2}^+$, to the considerable decrease in the Co−Co distance upon oxidation. This indicates that relaxation energies play a minor role in the relative order of the potentials. The solvation energies associated with the two redox pairs are much more important. However, even in the gas phase, the correct order of potentials is reproduced. These were obtained by the energy difference between the initial species and its oxidation product.

(54) (a) Dei Paggio, A. A.; Muetterties, E. L.; Heinekey, D. M.; Day, V. W.; Day, C. S. *Organometallics* **1986**, *5*, 575. (b) Albright, T. A; Burdett, J. K.; Whangbo, M. H. *Orbital Interaction in Chemistry*; Wiley: New York, 1985.

(55) For the failure of gas-phase calculations in predicting the redox behavior, see: Baik, M.; Ziegler, T.; Schauer C. K. *J. Am. Chem. Soc.* **2000**, *122*, 9143 and references therein.

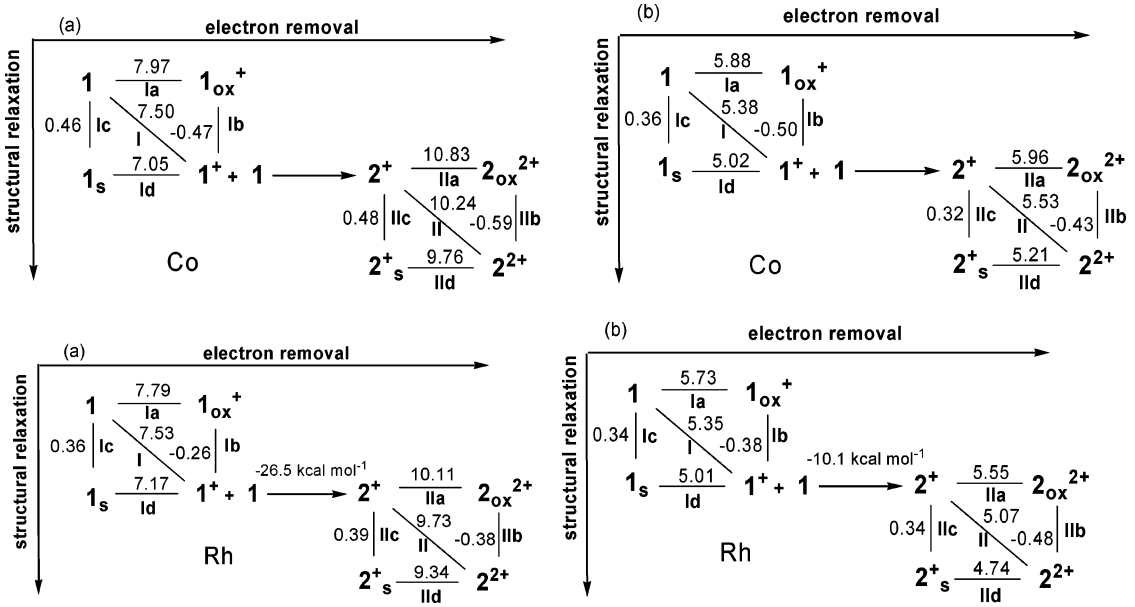

Figure 13. Energy-partition diagram (eV) for the oxidation of complexes $MCp(CO)_2$ (**1**) and $M_2Cp_2(CO)_4$ ($\mathbf{2}^+$), M = Co and Rh: (a) gas phase, (b) COSMO.

Let us now compare Co and Rh. In the Rh system, $\mathbf{2}^+$ (M = Rh) is easier to oxidize than the neutral complex **1** (M = Rh). If we look at the numbers for the $\mathbf{1} \rightarrow \mathbf{1}^+$ process, the differences between Co and Rh are negligible, but the same is not true for the $\mathbf{2}^+ \rightarrow \mathbf{2}^{2+}$ oxidation. Upon introduction of solvent effects, E°_2 drops from 10.24 to 5.53 V (still higher than E°_1) for Co, but from 9.73 to 5.07 V (now lower than E°_1) for Rh. Among the two terms defining the complete oxidation, the removal of one electron differs significantly from Co to Rh (5.96 vs 5.55 V from $\mathbf{2}^+ \rightarrow \mathbf{2_{ox}}^{2+}$ or 5.21 vs 4.74 from $\mathbf{2_s}^+ \rightarrow \mathbf{2}^{2+}$), while the structural relaxation term is almost the same (0.32 vs 0.34). This means that the energy of the SOMO for $[Rh_2Cp_2(CO)_4]^+$, the putative Rh analogue of $\mathbf{2}^+$, is higher than that of $\mathbf{2}^+$, though the two orbitals are similar and strongly M−M antibonding. This behavior arises from bonding factors. The overlap between the 4d orbitals of Rh is greater than that between the more contracted 3d orbitals of Co, pushing the Rh−Rh antibonding orbitals to higher energy. Furthermore, the d, s, and p contribution of Co is 50.4%, 2.5%, and 2.2%, respectively, whereas, for Rh, these numbers drop to 42.7%, 2.9%, and 0%. Since empty s and p orbitals will mix into the M−M σ^* in a bonding way, this effect is more relevant for Co, also helping to lower the energy of the SOMO. We are studying this problem computationally with related transition metal complexes to check the applicability of this interpretation.

Major Conclusions

(1) In a gentle electrolyte medium, 1-electron oxidation of $CoCp(CO)_2$ gives the reactive 17-electron radical cation $[CoCp(CO)_2]^+$.

(2) Rehybridization of the radical cation opens the metal center for reactions with a one- or two-electron donor. In the absence of strong donors, the radical reacts with $CoCp(CO)_2$, giving the dimer radical cation $[Co_2Cp_2(CO)_4]^+$, which may be further oxidized to the dimer dication $[Co_2Cp_2(CO)_4]^{2+}$. The fact that the neutral compound **1** acts as a nucleophile toward $\mathbf{1}^+$ is qualitatively explained by the known Lewis basicity of cobalt group complexes of the type $M(\eta^5\text{-}C_5R_5)(CO)L$.[56]

(3) The reaction of $[CoCp(CO)_2]^+$ with $CoCp(CO)_2$ constitutes a radical−substrate (R−S) dimerization process in which the R−S product, $[Co_2Cp_2(CO)_4]^+$, is observable by voltammetry. This appears to be the first direct confirmation of an R−S dimerization product. Such products have not been previously observed owing to the fact that they are normally more easily oxidized than the starting material itself.

(4) DFT calculations confirm that the LUMO of the dimer dication is Co−Co antibonding and show that the redox reaction $[Co_2Cp_2(CO)_4]^{2+} + e^- \rightarrow [Co_2Cp_2(CO)_4]^+$ leads to a lengthening of the metal−metal bond from 2.64 Å to 3.14 Å. The carbonyl ligands remain terminal.

(5) Calculations consistent with the fact that the $E_{1/2}$ of $[Co_2Cp_2(CO)_4]^{+/2+}$ is positive of the $E_{1/2}$ of $[CoCp(CO)_2]^{0/+}$ must take into account the solvation energies of the species involved.

Finally, we find it somewhat surprising that new and fundamentally different redox chemistry should emerge for the otherwise widely studied[57] half-sandwich compound $CoCp(CO)_2$ more than five decades after its initial report.[58] The present findings indicate that dramatically different chemistry may be found for the anodic oxidation of simple organometallic compounds in gentle media comprised of lower-polarity, weak-donor solvents with WCA-containing supporting electrolytes. We are in the process of exploring new organometallic cation radical chemistry based on these observations.

Acknowledgment. We gratefully acknowledge support by NSF (CHE-0092702 and CHE-0411703), by FCT (SFRH/BD/10535/2002), and by the Egyptian Ministry of Higher Education (CD-1904). A.N. wishes to thank Prof. R. Abdel-Hamid, A. Mostafa, and H. El-Sagher, Sohag University, Egypt, for their joint supervision of his Ph.D. work at the University of Vermont.

(56) Werner, J. *Angew. Chem., Int. Ed. Engl.* **1983**, *22*, 927.
(57) Kemmitt, R. D. W.; Russell, D. R. In *Comprehensive Organometallic Chemistry*; Wilkinson, G., Stone, F. G. A., Abel, E. W., Eds.; Pergamon Press: Oxford, 1982; Volume 5, pp 248 ff.
(58) Fischer, E. O.; Jira, R. *Z. Naturforsch.* **1955**, *B10*, 355.

Supporting Information Available: One table giving bond distances, τ angles, and electrostatic solvation energies for **1**, $\mathbf{1}^+$, $\mathbf{2}^+$, and $\mathbf{2}^{2+}$; two figures showing (a) simulated CV for oxidation of 0.3 mM **1** at 0.2 V s^{-1} and (b) IR spectra (syringe method) for bulk oxidation of **3**. This material is available free of charge via the Internet at http://pubs.acs.org.

JA0653775